HHS Public Access

Author manuscript

Nat Neurosci. Author manuscript; available in PMC 2015 January 01.

Published in final edited form as:

Nat Neurosci. 2014 July ; 17(7): 914–922. doi:10.1038/nn.3724.

Mechanical coupling maintains the fidelity of NMDA receptor-mediated currents

Rashek Kazi[1,2], **Jian Dai**[5], **Cameron Sweeney**[3,4], **Huan-Xiang Zhou**[5], and **Lonnie P. Wollmuth**[3,4]

[1]Graduate Program in Neuroscience, Stony Brook University, Stony Brook, NY 11794-5230

[2]Medical Scientist Training Program (MSTP), Stony Brook University, Stony Brook, NY 11794-5230

[3]Department of Neurobiology and Behavior, Stony Brook University, Stony Brook, NY 11794-5230

[4]Center for Nervous System Disorders, Stony Brook University, Stony Brook, NY 11794-5230

[5]Department of Physics and Institute of Molecular Biophysics, Florida State University, Tallahassee, FL 32306

Abstract

The fidelity of NMDA receptors (NMDARs) to integrate pre- and post-synaptic activity requires a match between agonist binding and ion channel opening. To address how agonist binding is transduced into pore opening in NMDARs, we manipulated the coupling between the ligand binding domain (LBD) and the ion channel by inserting residues in a linker between them. We find that a single residue insertion dramatically attenuates the ability of NMDARs to convert a glutamate transient into a functional response. This is largely due to a decreased likelihood for the channel to open and remain open. Computational and thermodynamic analyses suggest that insertions prevent the agonist-bound LBD from effectively pulling on pore lining elements, thereby destabilizing pore opening. Further, this pulling energy is more prominent in the GluN2 subunit. We conclude that an efficient NMDAR-mediated synaptic response relies on a mechanical coupling between the LBD and the ion channel.

Keywords

Synaptic transmission; ion channels; ionotropic glutamate receptors; molecular dynamics simulations; homology modeling; kinetic modeling; domain coupling

Address for correspondence: Dr. Lonnie P. Wollmuth, Dept. of Neurobiology & Behavior, Center for Nervous System Disorders, Stony Brook University, Stony Brook, New York 11794-5230, Tel: (631) 632-4186, Fax: (631) 632-6661, lonnie.wollmuth@stonybrook.edu.

Author Checklist

R.K., H-X. Z., and L.P.W. designed research; R.K. and C.S. carried out and analyzed the electrophysiology experiments; J.D. performed the computational studies including modeling and molecular dynamic simulations; R.K. carried out secondary structure predictions; R.K., J.D., H-X. Z., and L.P.W. wrote the paper.

INTRODUCTION

Rapid chemical signaling between cells in the nervous system requires a close temporal connection between the release of neurotransmitter and the activation of the neurotransmitter-gated receptor. To facilitate the efficiency of signaling, fast chemical synapses typically employ neurotransmitter-gated ion channels. These protein complexes contain both the neurotransmitter binding site and the ion channel that mediates the cellular response, thereby facilitating the conversion of transient neurotransmitter into an efficient signal. In all neurotransmitter-gated ion channels, including cys-loop[1,2], purinergic[3], and ionotropic glutamate receptors[4,5], the neurotransmitter binding site and the transmembrane domain harboring the ion channel are spatially remote, requiring the conformational changes occurring at the transmitter binding site to be tightly linked to those occurring in the ion channel, culminating in pore opening.

The majority of fast synaptic transmission in the central nervous system uses glutamate as a neurotransmitter. Neurotransmitter-gated or ionotropic glutamate receptors (iGluRs), including the NMDA, AMPA and kainate receptor subtypes, must overcome a unique challenge in converting transient glutamate into a synaptic response: iGluR subunits are composed of discrete, highly modular domains that are separated from each other by flexible regions[4,5]. The extracellular ligand-binding domain (LBD) shares homology with periplasmic binding proteins. It is structurally separated enough from other domains that LBDs from a variety of iGluR subtypes have been genetically isolated and crystallized in an assortment of ligand bound states[6–8]. The membrane embedded ion channel, on the other hand, shares homology with K^+ channels[9,10]. As is the case for any ligand-gated ion channel, the conformational changes that occur at the LBD must be transduced to channel opening in some fashion. Although the molecular basis for this process has been speculated upon[11,12], there is no evidence for how it occurs in an intact or full-length iGluR. Potential mechanisms of allosteric coupling may involve a mechanical pulling of the linkers[13,14], as in calcium-activated K^+ channels[15], or changes in residue interactions, as in cys-loop receptors[2].

NMDARs mediate plasticity in the nervous system by converting neuronal activity into changes in synaptic strength and connectivity[16]. These receptors efficiently integrate transient glutamate into a prolonged response. To address the coupling mechanism between the LBD and ion channel in NMDARs, we focused on a short polypeptide linker between the S2 segment of the LBD and the M3 transmembrane helix, the M3-S2 linker. In iGluRs, the M3 transmembrane helix, homologous to the TM2 or S6 segment in K^+ channels[5,9,10], is the main pore-forming segment and presumably contains elements that preclude ion flux in the closed state[5,17]. Using single molecule electrophysiological and computational approaches, we provide direct evidence that mechanical pulling is a significant component of NMDAR activation. The importance of this mechanism is highlighted by results showing that a single residue insertion in the M3-S2 linker nearly abolishes the ability of NMDARs to convert transient glutamate into a functional response. Further, NMDARs are obligate heterotetramers containing two glycine-binding GluN1 subunits and typically two glutamate-binding GluN2 subunits. We find that for robust pore opening to occur, the GluN2A subunits must transfer more energy and at an earlier time point than the GluN1

subunits. Therefore, NMDARs require mechanical coupling to efficiently convert transient glutamate into prolonged pore opening, a central feature of NMDARs in synaptic dynamics.

RESULTS

Fast synaptic-like activation of NMDARs

The glutamate transient in the synaptic cleft rises rapidly to a peak concentration of around 1 mM and then decays within several milliseconds[18]. We therefore rapidly applied glutamate (1 mM for 2 ms) to outside-out patches containing a single (wild type) or no more than two (insertion constructs) NMDARs in the continual presence of glycine (Fig. 1a–c). In response to this brief glutamate application, wild type NMDARs composed of GluN1/GluN2A showed frequent activity (Fig. 1a). This included a brief interval between the application of glutamate and the 1st opening of the ion channel as well as persistent channel activity, generally for many tens of milliseconds[19,20]. As is found for NMDAR-mediated synaptic responses, the sum of this individual activity showed a rapid rise (~5–6 ms) followed by a slower decay (~40 ms) (*lowest trace*, Fig. 1a)[21]. This profile of ion channel opening in response to transient glutamate contributes to the unique role of NMDARs to synaptic function.

The NMDAR-mediated synaptic profile is defined by the mechanism of ion channel opening following ligand binding[21]. The LBD is connected to the transmembrane domain through polypeptide linkers (Fig. 1d). We rapidly applied glutamate to NMDARs where a single glycine residue was inserted, adjacent to an endogenous glycine, in the M3-S2 linker (Fig. 1e) of either the GluN1 [GluN1(G648+1G)] (Fig. 1b) or GluN2A [GluN2A(G645+1G)] (Fig. 1c) subunit. These single glycines, inserted in the pathway between the LBD and the ion channel (Fig. 1d,e), dramatically attenuated the transduction of the transient glutamate signal as evidenced by an increased number of applications where no channel activity was detected (failures) and greatly truncated activity even when channels opened. Consequently, summed currents (Figs. 1b,c, *lowest traces*) showed peak amplitudes (Fig. 1f) and charge transfers (Fig. 1g) that were significantly reduced compared to those of wild type by about 70% for the GluN1 insertion and 90% for the GluN2A insertion. Thus, a single glycine introduced in the M3-S2 linker between the LBD and the ion channel of either GluN1 or GluN2A largely eliminates the ability of NMDARs to efficiently integrate the transient glutamate signal into a postsynaptic response.

Rapid and prolonged agonist applications to NMDARs

To begin addressing how a single glycine insertion in the M3-S2 linker impacts NMDAR activation, we recorded currents from outside-out patches exposed to longer pulses (1 s) of glutamate. These outside-out patches contained a single NMDAR. To maximize NMDAR activity, we transitioned to an external solution that was NaCl-based but at a higher pH (8.0) and contained high EDTA (1 mM) (see Online Methods).

In response to the long glutamate application, single wild type GluN1/GluN2A NMDARs were typically continually active (Fig. 2a, *upper two traces*), though certain activations were truncated (Fig. 2a, *third trace*), and some applications showed failures (18.3 ± 1.9%, mean ±

SEM). In contrast, NMDARs containing single glycine insertions in GluN1 (Fig. 2b) or GluN2A (Fig. 2c) showed dramatically reduced activity. In part, this arose because of a significantly increased failure rate (GluN1(G648+1G), 49.7 ± 6.6%, n = 6 patches, 244 applications; GluN2A(G645+1G), 47.1 ± 4.0%) (Fig. 2d) as well as a prolonged latency to 1st opening (GluN1/GluN2A, 57.7 ± 12 ms; GluN1(G648+1G), 106 ± 30 ms, n = 8 patches, 297 applications; & GluN2A(G645+1G), 311 ± 15.3 ms, n = 9 patches, 398 applications) (Fig. 2e). However, even when channels opened, activity was significantly truncated as indexed by the average open time when channels were active during an application (GluN1/GluN2A, 358.9 ± 85 ms; GluN1(G648+1G), 54.5 ± 9 ms; & GluN2A(G645+1G), 21.8 ± 5 ms) (Fig. 2f).

The effect of single glycine insertions on opening of the ion channel in response to glutamate – the increase in failure rates and in latencies to 1st opening as well as the decrease in open time per application – could arise via three general mechanisms. (1) These manipulations could dramatically alter the efficiency of agonist binding and/or the subsequent conformational changes in the LBD. Our data suggest that glycine insertions have limited effects on LBD function (Supplementary Fig. 1). (2) Alternatively, the glycine insertions could promote NMDAR desensitization, but this is unlikely since wild type and glycine-inserted constructs show comparable desensitization (Fig. 2g,h). (3) Finally, insertions in the M3-S2 linker could impede the coupling mechanism between the LBD and the ion channel.

As an initial test of this latter idea, we quantified the distribution of latencies to 1st opening (Fig. 2i–k). These distributions presumably reflect the occupancy of ligand-bound closed states that precede channel opening[22]. Therefore, if the coupling mechanism between the LBD and the ion channel is affected by these single glycine insertions, we would anticipate changes in these latency distributions. For wild type GluN1/GluN2A, the distribution was best fit by two exponential functions (Fig. 2i) (see Online Methods), which suggests that the channel traverses through multiple closed states prior to opening, consistent with proposed mechanisms of activation for NMDARs[19,23–25]. For both single glycine insertion constructs (Figs. 2j,k), the distributions of latencies were again best fit by two exponentials, suggesting that the fundamental mechanism of activation of these constructs is preserved. However, compared to GluN1/GluN2A, there were qualitative differences in the time constants and occupancies of each component (Fig. 2i–k). Indeed, both insertion constructs had increased time constants and decreased occupancy of the brief state while concomitantly increasing the occupancy of the long state. Further, these effects appeared greater for the GluN2A insertion construct than GluN1, suggesting that there may be subunit-specific differences in coupling[26,27]. Thus, insertions in the M3-S2 linker primarily preclude efficient energy coupling between the LBD and the ion channel.

Molecular dynamics simulations of NMDARs

To elucidate the molecular basis for the role of the M3-S2 linker in coupling the energetics of the LBD to the ion channel, we carried out molecular modeling and all-atom targeted molecular dynamics (MD) simulations. One potential problem with the insertion of a residue in the M3-S2 linker is that it may induce unanticipated changes in secondary structure. We

therefore used a homology model of the GluN1/GluN2A NMDAR[13] (Fig. 3a,b, *left panels*) and introduced single glycine residues either in GluN1 (Fig. 3a, *center panel*) or GluN2A (Fig. 3b, *center panel*) M3-S2 linker (see Online Methods). A comparison of the M3-S2 linker between wild type and insertion construct models (Fig. 3a,b, *right panels*) indicates that single glycine insertions add length without altering secondary structures (see also Supplementary Figs. 2 and 3). Further, to limit introducing additional flexibility, we inserted the single glycine adjacent to an endogenous glycine (Fig. 1e). Thus, the main structural effect of the single glycine insertion, at least in a putative closed state, is to add length to the M3-S2 linker.

We then performed targeted MD simulations of these modeled tetrameric NMDARs to address how glycine insertions affect the transition to an activated state (see Online Methods). In these simulations, the LBD was targeted to the agonist bound conformation[7,13] and then changes at the pore-lining M3 helices were monitored. For wild type GluN1/GluN2A, the M3 helices splay apart and are distant from the central-pore axis by the end of the simulations, due to the upward deflection of the lower lobe of the agonist-bound LBD that pulls on the M3 helices through the M3-S2 linkers[12–14]. The GluN2A subunit showed larger displacements of the M3 helix (Fig. 3c)[13]. These displacements presumably reflect the structural dynamics during activation of NMDARs, though the end-state of these simulations is not in the open state.

In the single glycine insertion constructs, the activated LBD also displaced the M3 helices (Fig. 3d,e) but the extent was limited (Fig. 3f). Further, compared to GluN1/GluN2A, the pore was more likely to stay in the resting conformation (≤ 1 Å pore radius) for the insertion constructs (Fig. 3g). All of these effects were more dramatic for the GluN2A insertion construct. Overall, these results suggest that, along the pathway to opening of the ion channel, the M3-S2 linker transduces the energetics of the LBD to pore-opening via a mechanical pulling mechanism, and a glycine insertion reduces the efficiency of the transduction, more so in the GluN1 subunit than in the GluN1 subunit.

Single insertions reduce equilibrium pore opening

If channel opening involves a mechanical pulling process, then insertions at different points between the LBD and M3 helix should reduce coupling, and thus pore opening. We therefore inserted individual glycine residues at different positions in the M3-S2 linker in either GluN1 (Fig. 4b) or GluN2A (Fig. 4e). For these and subsequent experiments, we recorded single-channel activity using the cell-attached configuration because it provides longer term recordings with low noise, simplifying detection of patches with a single channel, especially for constructs with low open probabilities. Further, recording large numbers of events allows for more accurate kinetic modeling of NMDAR activation[24,28]

At steady state, wild type GluN1/GluN2A NMDARs have an equilibrium open probability (P_o) of 0.67 ± 0.05 (n = 8 patches) (Fig. 4a, Table 1)[19,24,28–30]. Not unexpectedly, the single glycine insertion constructs previously tested (Figs. 1–3) reduced P_o significantly to 0.36 ± 0.06 (n = 8) for GluN1(G648+1G) (Fig. 4c,d) and even more dramatically to 0.08 ± 0.02 (n = 6) for GluN2A(G645+1G) (Fig. 4f,g). Glycines inserted at more membrane-proximal positions in the M3-S2 linker in GluN1 (Fig. 4b–d) or GluN2A (Fig. 4e–g) also significantly

reduced P_o. For GluN1, the reduction in P_o for the different positions was indistinguishable, whereas for GluN2A, the reduction for the membrane-proximal positions was significantly greater than that of the membrane-distal position (Fig. 4g, inset) (Supplementary Table 1). Thus, insertions in the M3-S2 linker at different points caused reductions in P_o, consistent with mechanical coupling between ligand binding and pore opening.

We initially used glycine insertions to test coupling because their absence of a side chain should prevent the introduction of new local interactions. Further, we inserted a glycine at a site where an endogenous glycine was already present (Fig. 1e), which should limit artificially introducing flexibility into the linker. Still, if pulling is important to pore opening, then insertions of different types of amino acids should, at minimum, reduce P_o. Indeed, like the glycine insertions, insertion of alanine or serine at GluN1(G648) or GluN2A(G645) (Supplementary Table 2) strongly reduced P_o. In fact, the reduction was greater than that observed for the glycine insertions. We do not know the basis for this additional reduction in gating but it may reflect unanticipated changes in local interactions. Overall, these results are consistent with the hypothesis that mechanical pulling is a significant component of pore opening in NMDARs.

Additional insertions further reduce pore opening

If pore opening is largely driven by mechanical pulling, additional insertions, which presumably make the M3-S2 linker longer, should further curtail pore opening. We therefore inserted multiple consecutive glycines (+2G and +4G) at GluN1(G648) (Fig. 5a) or GluN2A(G645) (Fig. 5b). Compared to the P_o values for the single glycine insertions at these sites, 0.36 for GluN1 and 0.08 for GluN2A (Fig. 4), the insertion of an additional glycine in GluN1 [GluN1(G648+2G)] (Fig. 5a) or GluN2A [GluN2A(G645+2G)] (Fig. 5b) resulted in a significantly lower P_o (0.16 ± 0.05, $n = 5$ & 0.008 ± 0.002, $n = 5$, respectively). The insertion of 4 glycines in GluN1 [GluN1(G648+4G)] (Fig. 5a) or GluN2A [GluN2A(G645+4G)] (Fig. 5b) also resulted in P_o values that were significantly less than their respective single glycine insertions (0.13 ± 0.02, $n = 4$ & 0.003 ± 0.001, $n = 6$, respectively) (Table 1). For GluN2A, the P_o values for the +2G and +4G constructs were significantly different ($p < 0.05$), whereas for GluN1 the difference was not statistically significant. One possibility for the lack of a significant decrease for GluN1 is that insertions beyond +2G may not result in the expected increases in linker length. Indeed, for insertions beyond +2G in GluN1 (Supplementary Fig. 2) and to a lesser extent in GluN2A (Supplementary Fig. 3), there were hints of new structural elements that might not increase the linker length as much as expected. Nevertheless, these results are consistent with the idea that pulling is required for efficient pore opening in NMDARs.

We also performed targeted MD simulations on NMDAR models containing the +4G insertions (Supplementary Fig. 4). Consistent with mechanical coupling, these additional insertions limited pore widening even more than the single glycine insertions (Supplementary Fig. 4d). We also found a striking parallel between pore radius derived from MD simulations and P_o (Fig. 5c–d), highlighting the relationship between these parameters.

Reductions in P_o must result from increases in mean closed time (MCT) and/or decreases in mean open time (MOT). Presumably, equivalent insertions in the different NMDAR

subunits could exert their effects on MCT and MOT in a qualitatively comparable manner. Indeed, this alternative seems likely given that NMDARs gate in a concerted manner[31]. Surprisingly, however, the effect of equivalent insertions in the different subunits was not comparable (Fig. 5e–f). In particular, single glycine insertions (+1G) in either GluN1 or GluN2A significantly increased MCT (8.5 ± 1.3 ms & 76.2 ± 27 ms, respectively) and reduced MOT (4.2 ± 0.5 ms & 4.2 ± 0.4 ms, respectively) relative to wild type MCT (3.8 ± 0.8 ms) and MOT (7.9 ± 0.9 ms). However, compared to +1G, four glycine insertions (+4G) in GluN2A further increased MCT (2300 ± 600 ms) but did not significantly increase MCT in GluN1 (12.4 ± 1.8 ms). On the other hand, +4G further decreased MOT in GluN1 (1.7 ± 0.1 ms) but not in GluN2A (3.7 ± 0.4 ms). Thus, it appears that pulling from the different subunits contributes to distinct features of pore opening with GluN2A mainly regulating the frequency of opening and GluN1 mainly regulating the duration of opening, though this distinction is by no means absolute. This idea is consistent with the prominent regulatory role of GluN2 in NMDAR activity[32,33].

Deletions of residues in the M3-S2 linker could also affect the mechanical coupling between the LBD and the ion channel. However, from homology modeling (Phyre and SWISS-MODEL), we often found that deletions in the M3-S2 linker altered local structures and led to ambiguous results from simulations (data not shown). Since interpreting the effects of insertions/deletions requires unaltered local structures and clear simulation results, we did not pursue the deletion experiments further.

Subunit-specific pulling energies during NMDAR activation

Subsequent to agonist binding, NMDARs undergo a series of kinetically resolvable transitions prior to pore opening (Fig. 2g–i)[20,23,24,28–31] (Fig. 6a). To discern how the pulling actions of the different subunits affect this activation sequence, we fit our cell-attached recordings to a kinetic model of NMDAR activation (Supplementary Figs. 5 and 6). Single glycine insertions in GluN1 (1.4 ± 0.2) (Fig. 6b) or GluN2A (0.7 ± 0.1) (Fig. 6c) significantly reduced the equilibrium constant (K_{eq}) of the opening isomerization, C_1−O_1, compared to wild type (2.6 ± 0.3) (Fig. 6a). In contrast, K_{eq} values for earlier transitions were only significantly reduced for GluN2A (C_3−C_2: 3.5 ± 0.4; C_2−C_1: 0.1 ± 0.02) (Fig. 6c) but not for GluN1 (C_3−C_2: 6.5 ± 0.8; C_2−C_1: 0.3 ± 0.03) (Fig. 6c) compared to wild type (C_3−C_2: 7.1 ± 0.8; C_2−C_1: 0.4 ± 0.03) (Supplementary Table 4).

To test the functional implications of these kinetic models, we used the derived rates for GluN1/GluN2A (Fig. 6d), GluN1(G648+1G)/GluN2A (Fig. 6e), and GluN1/GluN2A(G645+1G) (Fig. 6f) to simulate NMDAR-mediated currents (Fig. 6d–f, *lower panels*) in response to 2 ms glutamate applications, as in Figure 1 (Fig. 6d–f, *upper panels*). Simulated currents for insertion constructs, compared to wild type, showed reduced peak amplitudes (Fig. 6d–f) and charge transfers (Fig. 6g), which paralleled experimental outcomes. The simulations also captured the strong subunit-specific differences. One notable difference was that the simulated currents showed a slower rate of deactivation. This is most likely due to the differences in extracellular solutions[4] since the simulations were derived from single-channel experiments performed in a divalent-free, EDTA-containing media.

To quantify the energy by which the different linkers pull on the ion channel, we used the derived kinetic rates (Supplementary Table 4) to calculate the Gibbs free energy difference (ΔΔG) for each kinetic transition (Fig. 7a). From the linear fit to these plots, we determined a pulling factor (*k*) which quantifies the pulling strength along the linker during a given transition. At the concerted opening transition, C_1−O_1, the pulling factors for GluN1 and GluN2A were comparable (1.3 & 1.1 kcal/mol/nm, respectively) (Fig. 7b). In contrast, GluN2 exerts greater pulling energy during earlier transitions, C_3−C_2 and C_2−C_1 (Fig. 7b). Thus the different subunits pull on the ion channel with about equal veracity during the final pore opening transition (C_1−O_1). This is consistent with concerted gating in NMDARs with a rapid, but relatively uniform pore opening isomerization. On the other hand, prior to this pore opening transition, the GluN2 subunit is exerting significant energy and hence must undergo more extensive isomerization compared to GluN1. Indeed, the average GluN2A *k* across all transitions (1.6 ± 0.3 kcal/mol/nm) is greater than the average *k* for GluN1 (0.66 ± 0.3 kcal/mol/nm) by a factor of approximately 2.4. From our MD simulations, the GluN2A M3 helices at the level of the pore entrance were found to separate more (8.5 Å) than that of GluN1 (3.6 Å) by a factor of approximately 2.4 (Fig. 7c). Thus, subunit-specific pulling energy may account for the differences in M3 helix separation and suggests asymmetrical pre-open state conformational changes before concerted pore opening.

DISCUSSION

Our results indicate that the tight linkage between agonist binding and ion channel opening in NMDARs is critical to their ability to convert transient glutamate into a robust functional response. We propose that this linkage is mainly, though not exclusively, due to mechanical coupling between domains in which the LBD of the NMDAR subunits pulls on the pore-lining M3 helix, facilitating pore opening. Both the glycine-bound GluN1 and glutamate-bound GluN2 subunits pull on M3 with about equivalent energy to open the pore (C_1−O_1), but surprisingly the GluN2 subunit transduces more energy during earlier transitions (Fig. 7b). Thus, under synaptic conditions where the glycine-binding site is generally thought to be saturated, synaptically-released glutamate acts as a rate limiting step to pore opening.

The functional properties of NMDARs, including pore opening, are determined by the specific GluN2 subunit (GluN2A, 2B, 2C, 2D)[33,34]. While both GluN1 and GluN2A showed evidence of pulling, we find that pulling in GluN2A occurs earlier and is more dynamic (Fig. 7b). As such, varied pulling energetics across the GluN2 subunits may contribute to the diversity of NMDAR activity. Further, because the GluN2 subunit must transfer more energy, mutations in it would likely produce more dramatic pathological phenotypes. Indeed, compared to GluN1, a greater number of missense mutations in the GluN2A subunit have been associated with neurological diseases[35–37].

Although our results are consistent with a mechanical pulling model of channel opening[7,8,12–15], the nature of the mechanical components remains to be resolved. Indeed, mechanical forces could entail twisting or rocking components[38]. Further, it is possible for channel opening to depend on shuffling the interactions of residue side chains, as is found in pentameric channels[2,39,40]. Indeed, mutations along the coupling linkers in iGluRs impact the stability of activation and desensitization states but it is unclear how such mutations may

affect the dynamics of pore opening[4,41,42]. The availability of a full-length structure of NMDARs, as opposed to a homology model, would provide better insights into these questions.

Recently, several neurological pathologies were associated with inherited and *de novo* NMDAR mutations that alter channel opening. Indeed, missense mutations within the GluN1 and GluN2A linkers have been identified in patients diagnosed with epileptic aphasic syndromes (specifically, Landau–Kleffner syndrome) and intellectual disabilities[35,37]. Surprisingly, insertion and deletion mutations in GluN2A or GluN1 were found in patients exhibiting focal epilepsies or mental retardation coupled with hypotonia, respectively[35,36]. Thus, efficient mechanical coupling is vital to NMDAR function and disruption of this process can lead to devastating clinical pathologies.

ONLINE METHODS

Mutagenesis and heterologous expression

Mutations were made in rat GluN1a (NCBI Protein database accession no. P35439) or GluN2A (accession no. Q00959) via QuickChange site-directed mutagenesis (Stratagene, La Jolla, CA.)[30]. GluN1 and GluN2A cDNA constructs were cotransfected into mammalian human embryonic kidney 293 (HEK 293) cells along with a separate pEGFP-Cl vector at a ratio of 1:1:1 using X-tremeGene 9 (Roche). To improve cell survivability, transfected cells were bathed in media containing the GluN2A competitive antagonist DL-2-amino-5-phosphonopentanoic acid (APV; 100 μM) and magnesium (100 μM). All experiments were performed 12–48 hours post-transfection.

Single channel recordings

Single channel currents were recorded at room temperature using an integrating patch clamp amplifier (Axopatch 200B; Molecular Devices), analog filtered at 10 kHz (four-pole Bessel filter), and digitized between 25 and 50 kHz (ITC-16 interfaced with PatchMaster, HEKA). Our standard bath solution consisted of 150 mM NaCl, 2.5 mM KCl, and 10 mM HEPES (pH 8.0, NaOH). Patch pipettes (thick-wall, borosilicate, Sutter Instruments) were pulled and fire-polished achieving resistances between 3 and 30 MΩ when measured in the bath. For outside-out recordings, patch pipettes were filled with 140 mM KCl, 1 mM BAPTA, and 10 mM HEPES (pH 7.2, NaOH). At −100 mV, seal resistance ranged between 1 and 20 GΩ. Agonists were applied via a piezo driven double-barrel application pipette system with a 10%–90% rise time of 250–500 μs. For cell-attached recordings, patch pipettes were filled with the standard bath solution as well as 1 mM glutamate and 0.1 mM glycine. 1 mM EDTA was added to minimize gating effects of divalents[4,24,28]. Inward currents were elicited by applying a pipette potential of +100 mV.

For outside-out patches, we used two different protocols: either a brief (2 ms, Fig. 1) or a long (1 s, Fig. 2) application. Different patches were used for the different protocols. For the brief protocol, the baseline barrel contained 150 mM NaCl, 2.5 mM KCl, 0.1 mM glycine, 0.02 mM EDTA, 0.5 mM $CaCl_2$, and 10 mM HEPES (pH 7.3, NaOH) while the test barrel contained the same solution with added 1 mM glutamate. This solution approximates a

physiological extracellular solution with minimized zinc[19]. Patches were held at −70 mV. Glutamate was applied for 2 ms every 4 seconds. After 25–50 consecutive brief applications, glutamate was applied for 1 s approximately 5–10 times to test whether activity arose from a single channel. For GluN1/GluN2A, which has a high open probability (~0.7), no analyzed patches contained more than one channel. For the insertion constructs, which have a much lower open probability, it was difficult to ensure that activity was only from one channel. Nevertheless, we estimate that most recordings showed activity from 1, and at most 2, channels. The 2 ms and 1 s protocols were alternated until activity was no longer detectable.

For the long protocol (Fig. 2), the baseline barrel contained 150 mM NaCl, 2.5 mM KCl, 0.1 mM glycine, 1 mM EDTA, and 10 mM HEPES (pH 8.0, NaOH) while the test barrel contained the same solution with added 1 mM glutamate. Patches were held at −100 mV. Glutamate was applied for 1 s and pulses were delivered every 3 seconds to allow for recovery from desensitization. Because of the greater number of events collected for these experiments, we are more confident that patches contained a single channel.

Summation of channel activity from brief applications

For the brief application recordings, the lowest number of consecutive applications was 25. Numerous patches contained more than 25 consecutive applications, but to avoid bias, we analyzed these data in sets of 25 consecutive applications. Briefly, each patch was divided into separate sets of 25 consecutive applications. A set of 25 consecutive applications, which contained failures, was summed. The resultant summed current for each set was then averaged with the summed currents of the other sets of 25 current applications for that patch. For example, if there were 100 total applications recorded from a single patch, the currents from applications 1 through 25 would be summed and count as a single set. This would be repeated for each subsequent set of 25 applications resulting in 4 sets. The 4 sets for this patch would be averaged. The resulting averaged current, referred to as the summed current profile, for each patch was used for statistical analysis. Explicitly, the number of patches, applications, and sets were: GluN1/GluN2A: 5 patches, 250 applications, and 10 sets; GluN1(G648+1G)/GluN2A: 3 patches, 725 applications, and 29 sets; and GluN1/GluN2A(G645+1G): 2 patches, 475 applications, and 19 sets. The average summed currents for each patch were analyzed for peak amplitude and charge transfer. Charge transfer was the total charge integral following agonist application.

Single channel analysis from long applications

For long applications (1 s), the number of applications per patch ranged from 20–180. Briefly, data was exported from PatchMaster to QuB (http://www.qub.buffalo.edu) for analysis. Applications displaying significant amounts of noise were removed (~5–10% of applications). After data processing, the segmental k-means (SKM) algorithm was run to idealize the data (with a dead time of 0.020 ms) using a two state model (1 closed, 1 open)[43]. The idealized data was then manually scanned to remove false events.

Failure to open—In some instances, agonist application showed no discernible NMDAR mediated currents either during or after the removal of glutamate[19,44]. These instances are referred to as failures. % failures were calculated as:

$$\% \textit{ failures} = 100 * (\#\textit{ of failures}/\#\textit{ of total applications})$$

Latency to 1st opening—Durations from the start of an application to the first idealized open event were reported. We further manually checked each pulse to ensure that latencies reported were to properly idealized events (as opposed to misclassified events).

Latency to 1st opening times were pooled and imported into ChanneLab2 (Synaptosoft). The latencies were binned at ~ 60 μs intervals and histograms displaying number of events as a function of latency to 1st opening were generated. The cumulative histogram was fit by multiple exponential functions. Exponential components were added until the log likelihood could not be further improved. All constructs were best fit by 2 components as the addition of a 3rd component did not improve the log likelihood value.

Channel open time—To characterize the effect of insertions on the amount of time channels spent in the open state, we calculated the average open time. For each application with activity, the total open time was calculated from the idealization tool in QuB. These values were averaged for a given patch to yield the average open time. This value reflects the average amount of time the channel spends in the open state for an individual patch and was used for further statistical analyses. Note that the average open time is distinct from mean open time, which is the average amount of time the channel spends in the open state for a single opening event.

Secondary structure prediction and homology modeling

Insertions and deletion are presumed to alter the length of the M3-S2 linker. Alternatively, these manipulations may significantly perturb local secondary structures. We used two general approaches to test for the structural effects induced by our manipulations: homology modeling using servers (PHYRE/SWISS-MODEL)[45,46] and homology modeling using MODELLER[47]. The modeling servers provide a unique advantage because they incorporate secondary structure prediction (PSI-PRED, SSPro, JNet, and Disopred) in the modeling algorithm[45]. Models of the insertion constructs were overlaid with wild type models to qualitatively detect secondary structural changes.

Computational models were based on a model structure of GluN1/GluN2A[13]. To insert residues into this full-length NMDAR model, we initially removed a few residues around the insertion point to create a gap in the wild type GluN1/GluN2A model and filled this gap with residues that correspond to the primary sequence of the mutated receptor. For example, for the model of GluN1(G648+1G)/GluN2A, with the insertion point between G648 and I649 in the GluN1 subunit, residues T647 and G648 were removed to create a gap; then this gap was filled in by residues T647, G648 and G648+1G. The resultant sequence became T647, G648, G648+1G, and I649. GluN2A subunits were left intact for the GluN1(G648+1G)/GluN2A model. Other insertion constructs were obtained in a similar fashion. All modeling for MD simulations was done using MODELLER[47].

All-atom molecular dynamics simulations

Molecular dynamics (MD) simulations were performed for a specific subset of constructs: GluN1/GluN2A, GluN1(G648+1G)/GluN2A, GluN1(G648+4G)/GluN2A, GluN1/GluN2A(G645+1G), and GluN1/GluN2A(G645+4G). Each model was independently energy minimized in vacuum, with a fixed backbone, for 2000 steps. The receptor was then incorporated into a lipid POPC bilayer. Lipid and water molecules that overlapped with the protein were subsequently removed. Ions were added to make the salt concentration of the system equal to 150 mM NaCl. System preparations were conducted using VMD[48]. After minimization, a simulation was run for 1 ns with protein backbone harmonically restrained at their initial positions using a 20 kcal/mol/A^2 force constant.

The targeted molecular dynamics simulation for each structure was performed similarly to what has been done for wild type receptors[13,14]. Briefly, the root mean square deviation (RMSD) values of the C-α atoms of the LBDs in our simulations were forced to gradually decrease to zero, with respect to the agonist-bound structure of the wild type GluN1/GluN2A LBD dimer (PDB ID: 2A5T)[7]. For WT simulations, the target LBD contains residues T378 to T419, P434 to K525 and I646 to C780 in GluN1 and N385 to S519 and V643 to C781 in GluN2A; for simulations of GluN1 insertion constructs, the target LBD contains residues T378 to T419, P434 to K525 and I649 to C780 in GluN1 while residues in GluN2A subunits remain the same as in the WT simulation; for simulations of GluN2A insertion constructs, the target LBD contains residues N385 to S519 and L646 to C781 in GluN2A while residues in GluN1 subunits remain the same as in the WT simulation.

All simulations were done using NAMD 2.9[49]. The simulation parameters for all structures were the same as those used for the simulation of the wild type receptor[13]. Each simulation was carried out for 65 ns using the CHARMM27 force field[50]. During the first 20 ns, the LBD slowly transformed to the conformation of the activated state. Pore radius was calculated using the HOLE program[51]. Frames which showed pore radii of < 1 Å were categorized as “pore collapsed”. % pore collapse was calculated as the # pore collapse frames/total # frames. This was calculated for the last 45 ns (using 900 frames) of the simulation.

Single channel analysis for cell-attached patches

Analysis of single-channel records was comparable to Kazi, et. al[30]. Recordings of GluN1/GluN2A receptors consisted of long clusters of activity separated by seconds-long periods of inactivity, simplifying detection of multiple channels in the patch[24,28]. For these recordings, the relatively high open probability (P_o) and duration of recordings (~60,000–600,000 events) indicated that we were recording from single-channel patches.

For certain insertion constructs, the P_o was extremely low which made single-channel patch detection difficult. First, many patches were recorded but excluded during analysis because of obvious simultaneous openings of multiple channels. Of the remaining patches, only several minutes-long recordings without any apparent simultaneous openings were further analyzed. Of the single-channel P_o values tabulated, the lowest was 0.002 for GluN1/GluN2A(G645+4G). If the patch contained two active channels of equivalent open

probability, then a double-channel opening would be expected approximately once every 500 events[30,52]. Of our records, only 4 of 103 on-cell patches showed less than 99% confidence in single channel activity.

Kinetic modeling was performed on the idealized data of an entire record. Equilibrium kinetic modeling was done using the maximum interval likelihood (MIL) algorithm (dead time of 0.024 ms). Models were built by increasing open and closed states until log-likelihood (LL) values improved by less than 10 LL units or if the next added state resulted in a state occupancy of 0%[30,53]. Kinetic models of NMDAR gating activation have been proposed to contain approximately 5 closed states and more than one open state[23,24,28,31]. We used a linear, fully-liganded model containing 3 closed states, 2 desensitized states, and 2 open states[23,30,53]. Time constants and the relative areas of each component, the transition rate constants (k_f & k_r), as well as mean closed time (MCT) and mean open time (MOT) were averaged for each construct and compared with each other.

Current simulations were performed as in[54]. Briefly, simulations were performed using QuB software using 200 channels for GluN1/GluN2A, 100 channels for GluN1(G648+1G)/GluN2A, and 100 channels for GluN1/GluN2A(G645+1G). Because the kinetic rates were calculated at equilibrium, it could not account for the failure rate of channel opening. Therefore, the difference in channel number is to account for the failure rate as approximated in Figure 2. Each channel was given a single-channel amplitude of 7.5 pA. The simulated pulse consisted of a fully liganded square pulse lasting 2 ms during a 2 s recording (250 ms prepulse). Two consecutive ligand binding steps were connected to the C_3 gating step (Fig. 6), with glutamate binding and unbinding constants of 1.7×10^7 M^{-1} s^{-1} and 60 s^{-1}, respectively.

Thermodynamic analysis

To define the thermodynamic impact of decoupling the LBD from the ion channel, we characterized the free energy change for each kinetic transition. We quantified the Gibbs free energy difference (ΔΔG) between wild type and insertion constructs for each activation transition (C_3−C_2, C_2−C_1, C_1−O_1):

$$\Delta G = -RTln(K_{eq}) \quad \text{Eq. 1}$$

$$\Delta\Delta G = \Delta G_{mut} - \Delta G_{WT} \quad \text{Eq. 2}$$

Statistics

Data analysis and statistics was performed using IgorPro (WaveMetrics), QuB, Excel (Microsoft), PyMol, VMD, and ChanneLab2 (Synaptosoft). Unless otherwise noted, macroscopic and microscope current amplitudes and single-channel properties are presented as mean ± SEM. We used a two-tailed Student's t-test to test significant differences between specific properties between different constructs. Multiple comparisons were not made because we are primarily interested in whether specific properties between two specific constructs differ from one another (i.e., comparing only open probability between only

GluN1/GluN2A and GluN1(G648+1G)/GluN2A), instead of trying to discern the overall difference among multiple comparisons. Unless otherwise noted, statistical significance was set at $p < 0.05$.

Unless otherwise indicated, a significant difference is indicated relative either to GluN1/GluN2A (*); to like constructs (e.g., single glycine insertions) between subunits [e.g., GluN1(G648+1G)/GluN2A versus GluN1/GluN2A(G645+1G)] (#); or to the single glycine insertions within subunits [e.g., GluN1(G648+1G)/GluN2A versus GluN1(G648+4G)/GluN2A] (^) ($p < 0.05$, two-tailed Student's t-test, unpaired).

No statistical test was run to determine sample size *a priori*. The sample size we chose was similar to those used in previous publications. Blinding and randomization were not necessary.

Supplementary Material

Refer to Web version on PubMed Central for supplementary material.

Acknowledgments

We thank Drs. James Howe and Claudio Grosman and Quan Gan for helpful discussions and/or comments on the manuscript, and Janet Allopenna and Melissa Daniel for technical assistance. This work was supported by Grants MH066892 (to LPW) and GM088187 (to HXZ) and Predoctoral Fellowship NS077541 (to RK) from the National Institutes of Health. The authors thank XSEDE for providing computational resources through grant TG-MCB130127 on TACC Stampede.

REFERENCES

1. Miyazawa A, Fujiyoshi Y, Unwin N. Structure and gating mechanism of the acetylcholine receptor pore. Nature. 2003; 423:949–955. [PubMed: 12827192]
2. Dacosta CJ, Baenziger JE. Gating of pentameric ligand-gated ion channels: structural insights and ambiguities. Structure. 2013; 21:1271–1283. [PubMed: 23931140]
3. Hattori M, Gouaux E. Molecular mechanism of ATP binding and ion channel activation in P2X receptors. Nature. 2012; 485:207–212. [PubMed: 22535247]
4. Traynelis SF, et al. Glutamate receptor ion channels: structure, regulation, and function. Pharmacol Rev. 2010; 62:405–496. [PubMed: 20716669]
5. Sobolevsky AI, Rosconi MP, Gouaux E. X-ray structure, symmetry and mechanism of an AMPA-subtype glutamate receptor. Nature. 2009; 462:745–756. [PubMed: 19946266]
6. Mayer ML. Structure and mechanism of glutamate receptor ion channel assembly, activation and modulation. Curr Opin Neurobiol. 2011
7. Furukawa H, Singh SK, Mancusso R, Gouaux E. Subunit arrangement and function in NMDA receptors. Nature. 2005; 438:185–192. [PubMed: 16281028]
8. Armstrong N, Gouaux E. Mechanisms for activation and antagonism of an AMPA-sensitive glutamate receptor: crystal structures of the GluR2 ligand binding core. Neuron. 2000; 28:165–181. [PubMed: 11086992]
9. Wo ZG, Oswald RE. Unraveling the modular design of glutamate-gated ion channels. Trends Neurosci. 1995; 18:161–168. [PubMed: 7539962]
10. Wood MW, VanDongen HM, VanDongen AM. Structural conservation of ion conduction pathways in K channels and glutamate receptors. Proc Natl Acad Sci U S A. 1995; 92:4882–4886. [PubMed: 7761417]
11. Hansen KB, Yuan H, Traynelis SF. Structural aspects of AMPA receptor activation, desensitization and deactivation. Curr Opin Neurobiol. 2007; 17:281–288. [PubMed: 17419047]

12. Jin R, Banke TG, Mayer ML, Traynelis SF, Gouaux E. Structural basis for partial agonist action at ionotropic glutamate receptors. Nat Neurosci. 2003; 6:803–810. [PubMed: 12872125]
13. Dai J, Zhou HX. An NMDA receptor gating mechanism developed from MD simulations reveals molecular details underlying subunit-specific contributions. Biophys J. 2013; 104:2170–2181. [PubMed: 23708357]
14. Dong H, Zhou HX. Atomistic mechanism for the activation and desensitization of an AMPA-subtype glutamate receptor. Nat Commun. 2011; 2:354. [PubMed: 21673675]
15. Niu X, Qian X, Magleby KL. Linker-gating ring complex as passive spring and Ca(2+)-dependent machine for a voltage- and Ca(2+)-activated potassium channel. Neuron. 2004; 42:745–756. [PubMed: 15182715]
16. Citri A, Malenka RC. Synaptic plasticity: multiple forms, functions, and mechanisms. Neuropsychopharmacology. 2008; 33:18–41. [PubMed: 17728696]
17. Chang HR, Kuo CC. The activation gate and gating mechanism of the NMDA receptor. J Neurosci. 2008; 28:1546–1556. [PubMed: 18272676]
18. Clements JD, Lester RA, Tong G, Jahr CE, Westbrook GL. The time course of glutamate in the synaptic cleft. Science. 1992; 258:1498–1501. [PubMed: 1359647]
19. Erreger K, Dravid SM, Banke TG, Wyllie DJ, Traynelis SF. Subunit-specific gating controls rat NR1/NR2A and NR1/NR2B NMDA channel kinetics and synaptic signalling profiles. J Physiol. 2005; 563:345–358. [PubMed: 15649985]
20. Gibb AJ, Colquhoun D. Glutamate activation of a single NMDA receptor-channel produces a cluster of channel openings. Proc Biol Sci. 1991; 243:39–45. [PubMed: 1708142]
21. Lester RA, Clements JD, Westbrook GL, Jahr CE. Channel kinetics determine the time course of NMDA receptor-mediated synaptic currents. Nature. 1990; 346:565–567. [PubMed: 1974037]
22. Pallotta BS. Calcium-activated potassium channels in rat muscle inactivate from a short-duration open state. J Physiol. 1985; 363:501–516. [PubMed: 2410610]
23. Auerbach A, Zhou Y. Gating reaction mechanisms for NMDA receptor channels. J Neurosci. 2005; 25:7914–7923. [PubMed: 16135748]
24. Schorge S, Elenes S, Colquhoun D. Maximum likelihood fitting of single channel NMDA activity with a mechanism composed of independent dimers of subunits. J Physiol. 2005; 569:395–418. [PubMed: 16223763]
25. Howe JR, Cull-Candy SG, Colquhoun D. Currents through single glutamate receptor channels in outside-out patches from rat cerebellar granule cells. J Physiol. 1991; 432:143–202. [PubMed: 1715916]
26. Sobolevsky AI, Prodromou ML, Yelshansky MV, Wollmuth LP. Subunit-specific contribution of pore-forming domains to NMDA receptor channel structure and gating. J Gen Physiol. 2007; 129:509–525. [PubMed: 17504910]
27. Talukder I, Borker P, Wollmuth LP. Specific sites within the ligand-binding domain and ion channel linkers modulate NMDA receptor gating. J Neurosci. 2010; 30:11792–11804. [PubMed: 20810899]
28. Popescu G, Auerbach A. Modal gating of NMDA receptors and the shape of their synaptic response. Nat Neurosci. 2003; 6:476–483. [PubMed: 12679783]
29. Talukder I, Wollmuth LP. Local constraints in either the GluN1 or GluN2 subunit equally impair NMDA receptor pore opening. J Gen Physiol. 2011; 138:179–194. [PubMed: 21746848]
30. Kazi R, et al. Asynchronous movements prior to pore opening in NMDA receptors. J Neurosci. 2013; 33:12052–12066. [PubMed: 23864691]
31. Banke TG, Traynelis SF. Activation of NR1/NR2B NMDA receptors. Nat Neurosci. 2003; 6:144–152. [PubMed: 12524545]
32. Siegler Retchless B, Gao W, Johnson JW. A single GluN2 subunit residue controls NMDA receptor channel properties via intersubunit interaction. Nat Neurosci. 2012; 15:406–413. S1-2. [PubMed: 22246434]
33. Paoletti P, Bellone C, Zhou Q. NMDA receptor subunit diversity: impact on receptor properties, synaptic plasticity and disease. Nat Rev Neurosci. 2013; 14:383–400. [PubMed: 23686171]

34. Yuan H, Hansen KB, Vance KM, Ogden KK, Traynelis SF. Control of NMDA receptor function by the NR2 subunit amino-terminal domain. J Neurosci. 2009; 29:12045–12058. [PubMed: 19793963]
35. Hamdan FF, et al. Excess of de novo deleterious mutations in genes associated with glutamatergic systems in nonsyndromic intellectual disability. Am J Hum Genet. 2011; 88:306–316. [PubMed: 21376300]
36. Lemke JR, et al. Mutations in GRIN2A cause idiopathic focal epilepsy with rolandic spikes. Nat Genet. 2013; 45:1067–1072. [PubMed: 23933819]
37. Lesca G, et al. GRIN2A mutations in acquired epileptic aphasia and related childhood focal epilepsies and encephalopathies with speech and language dysfunction. Nat Genet. 2013; 45:1061–1066. [PubMed: 23933820]
38. Yao Y, Belcher J, Berger AJ, Mayer ML, Lau AY. Conformational Analysis of NMDA Receptor GluN1, GluN2, and GluN3 Ligand-Binding Domains Reveals Subtype-Specific Characteristics. Structure. 2013; 21:1788–1799. [PubMed: 23972471]
39. Purohit P, Mitra A, Auerbach A. A stepwise mechanism for acetylcholine receptor channel gating. Nature. 2007; 446:930–933. [PubMed: 17443187]
40. Lee WY, Sine SM. Principal pathway coupling agonist binding to channel gating in nicotinic receptors. Nature. 2005; 438:243–247. [PubMed: 16281039]
41. Jones KS, VanDongen HM, VanDongen AM. The NMDA receptor M3 segment is a conserved transduction element coupling ligand binding to channel opening. J Neurosci. 2002; 22:2044–2053. [PubMed: 11896144]
42. Yelshansky MV, Sobolevsky AI, Jatzke C, Wollmuth LP. Block of AMPA receptor desensitization by a point mutation outside the ligand-binding domain. J Neurosci. 2004; 24:4728–4736. [PubMed: 15152033]
43. Qin F, Auerbach A, Sachs F. A direct optimization approach to hidden Markov modeling for single channel kinetics. Biophys J. 2000; 79:1915–1927. [PubMed: 11023897]
44. Gibb AJ, Colquhoun D. Activation of N-methyl-D-aspartate receptors by L-glutamate in cells dissociated from adult rat hippocampus. J Physiol. 1992; 456:143–179. [PubMed: 1293277]
45. Kelley LA, Sternberg MJ. Protein structure prediction on the Web: a case study using the Phyre server. Nat Protoc. 2009; 4:363–371. [PubMed: 19247286]
46. Bordoli L, et al. Protein structure homology modeling using SWISS-MODEL workspace. Nat Protoc. 2009; 4:1–13. [PubMed: 19131951]
47. Sali A, Blundell TL. Comparative protein modelling by satisfaction of spatial restraints. J Mol Biol. 1993; 234:779–815. [PubMed: 8254673]
48. Humphrey W, Dalke A, Schulten K. VMD: visual molecular dynamics. J Mol Graph. 1996; 14:33–38. 27-8. [PubMed: 8744570]
49. Phillips JC, et al. Scalable molecular dynamics with NAMD. J Comput Chem. 2005; 26:1781–1802. [PubMed: 16222654]
50. Mackerell AD Jr, Feig M, Brooks CL 3rd. Extending the treatment of backbone energetics in protein force fields: limitations of gas-phase quantum mechanics in reproducing protein conformational distributions in molecular dynamics simulations. J Comput Chem. 2004; 25:1400–1415. [PubMed: 15185334]
51. Smart OS, Goodfellow JM, Wallace BA. The pore dimensions of gramicidin A. Biophys J. 1993; 65:2455–2460. [PubMed: 7508762]
52. Colquhoun D, Hawkes AG. Stochastic properties of ion channel openings and bursts in a membrane patch that contains two channels: evidence concerning the number of channels present when a record containing only single openings is observed. Proc R Soc Lond B Biol Sci. 1990; 240:453–477. [PubMed: 1696014]
53. Kussius CL, Popescu GK. Kinetic basis of partial agonism at NMDA receptors. Nat Neurosci. 2009; 12:1114–1120. [PubMed: 19648915]
54. Talukder I, Kazi R, Wollmuth LP. GluN1-specific redox effects on the kinetic mechanism of NMDA receptor activation. Biophys J. 2011; 101:2389–2398. [PubMed: 22098737]

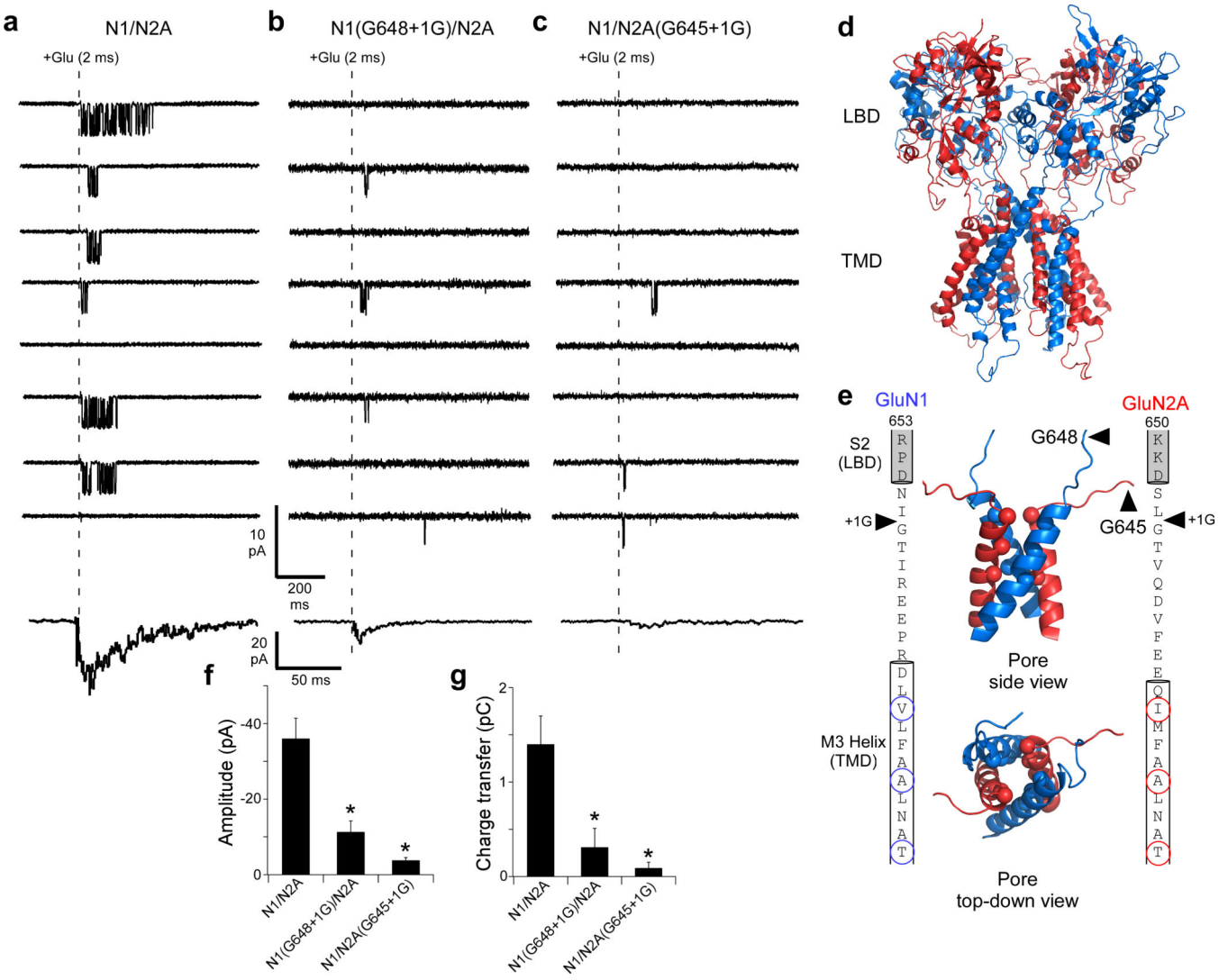

Figure 1. Single glycine insertions in either the GluN1 or GluN2A M3-S2 linker eliminates the fidelity of NMDAR-mediated currents

(**a–c**) *Top*, current traces (8 total; sampled at 25 kHz, displayed at 0.7 kHz) from outside-out patches in response to a brief application (2 ms, dashed line) of glutamate (1 mM) for GluN1/GluN2A (**a**), GluN1(G648+1G)/GluN2A (**b**), or GluN1/GluN2A(G645+1G) (**c**). Currents were recorded in the continual presence of glycine (0.1 mM). For GluN1/GluN2A, all patches contained exactly one channel but for the insertion constructs there were ≤ 2 channels. *Lowest trace*, summed current profile for individual patches (See Online Methods). Current profiles are the average of currents summed over 25 consecutive applications, including applications with no detectable openings (failures). Total applications & sets averaged: GluN1/GluN2A, 50 & 2; GluN1(G648+1G)/GluN2A, 300 & 12; GluN1/GluN2A(G645+1G), 225 & 9.

(**d**) Model structure of a GluN1(*blue*)/GluN2A(*red*) NMDAR[13].

(**e**) *Inner panels*, side (*top*) and top-down (*bottom*) view of the pore, formed by the M3 transmembrane helices. Spheres indicate α-carbons presumed to form the NMDAR gate[5,17]: top-to-bottom: GluN1(V638)/GluN2A(I635); GluN1(A634)/GluN2A(A631); and

GluN1(T630)/GluN2A(T627). *Outer panels*, Sequence of the M3-S2 linkers and adjoining M3 transmembrane helices and S2 segments for GluN1 (*left*) and GluN2A (*right*). Helical cut-offs are based on the NMDAR model. Arrowheads indicate sites of glycine insertion. Circles (spheres in structure) highlight gate-forming residues.

(**f & g**) Mean (± SEM) peak amplitude (**f**) and charge transfer (**g**) for summed currents (**a–c**, *bottom traces*); GluN1/GluN2A (n = 5 patches, 10 sets), GluN1(G648+1G)/GluN2A (n = 3 patches, 29 sets), GluN1/GluN2A(G645+1G) (n = 2 patches, 19 sets). * indicates a significant difference relative to GluN1/GluN2A ($p < 0.05$, two-tailed Student's t-test, unpaired).

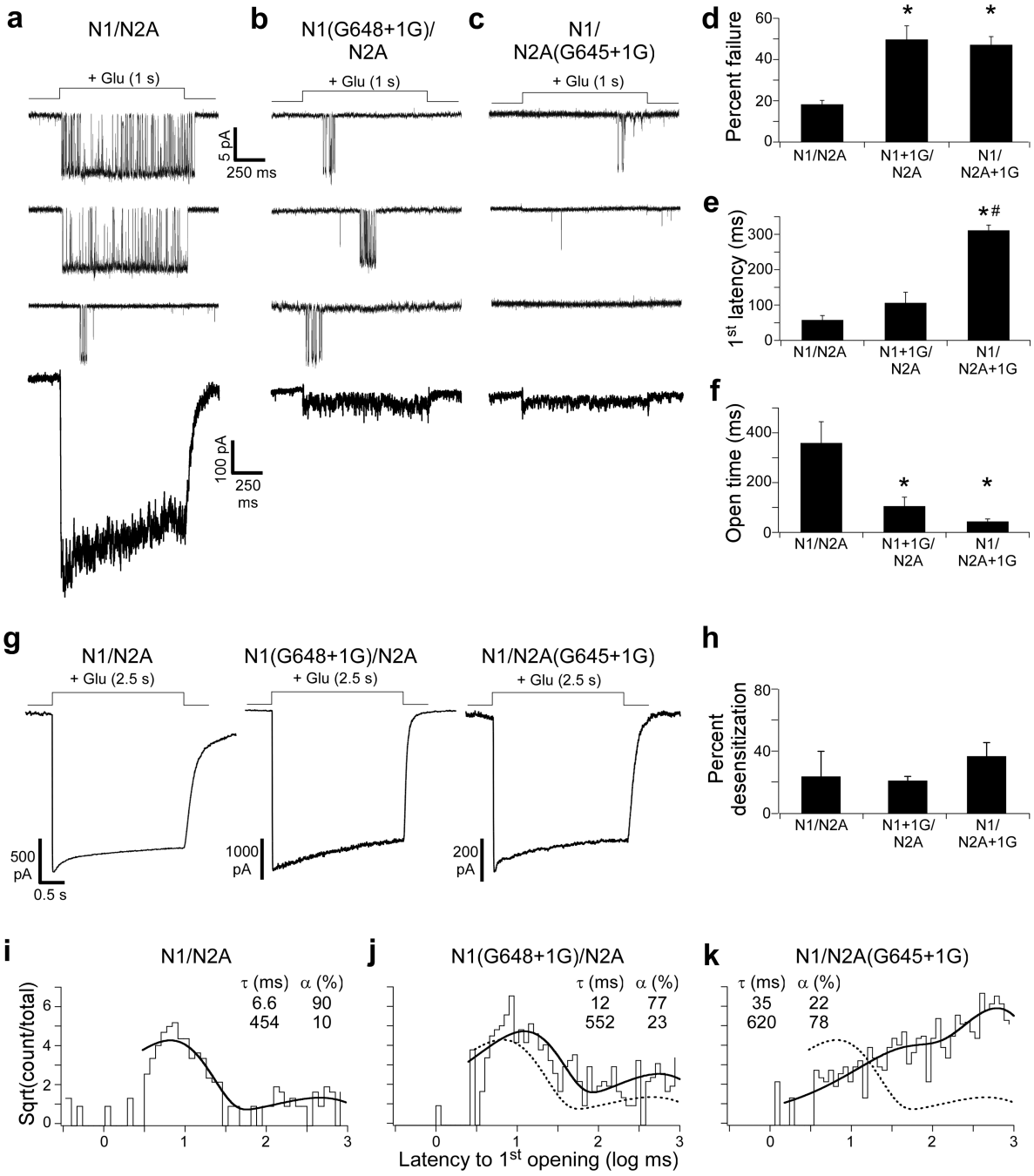

Figure 2. Single glycine insertions in the M3-S2 linkers increase failure rate and latency to 1st opening and reduce channel open time

(**a–c**) *Top*, Current traces (3 total) from outside-out patches in response to long applications (1 s) of glutamate (1 mM) for GluN1/GluN2A (**a**), GluN1(G648+1G)/GluN2A (**b**), or GluN1/GluN2A(G645+1G) (**c**). Pulses delivered approximately every 3 seconds. Currents were recorded in the continual presence of glycine (0.1 mM) and sampled at 50 kHz (shown at ~ 1 kHz). All patches contained a single channel. *Lowest trace*, current profile after summing 100 consecutive sweeps.

(**d–f**) Mean (± SEM) percent failure (**d**), latency to 1st channel opening (**e**), and open time (**f**) for GluN1/GluN2A (n ≥ 5 patches), GluN1(G648+1G)/GluN2A (n ≥ 6 patches), and GluN1/GluN2A(G645+1G) (n ≥ 8 patches). Open time (**f**) is the average time spent in the open state per application with openings (see Online Methods). A significant difference is indicated either relative to GluN1/GluN2A (*) or to GluN1(G648+1G)/GluN2A (#) ($p < 0.05$, two-tailed Student's t-test, unpaired).

(**g & h**) Insertions do not affect desensitization.

(**g**) Whole-cell current recordings in response to a 2.5 s glutamate (1 mM) application.

(**h**) Mean (± SEM, n ≥ 3) percent desensitization. Values were not statistically different.

(i–k) Cumulative distribution of latency to 1st opening for GluN1/GluN2A (**i**, 244 applications), GluN1(G648+1G)/GluN2A (**j**, 297 applications), and GluN1/GluN2A(G645+1G) (**k**, 388 applications) (latencies derived from records in **a–f**). Distributions were best fit by the sum of two exponentials (thick line) with time constants (τ, ms) and occupancies (α, %) shown. Dashed line in **j** and **k** is the best fit for GluN1/GluN2A in **i**.

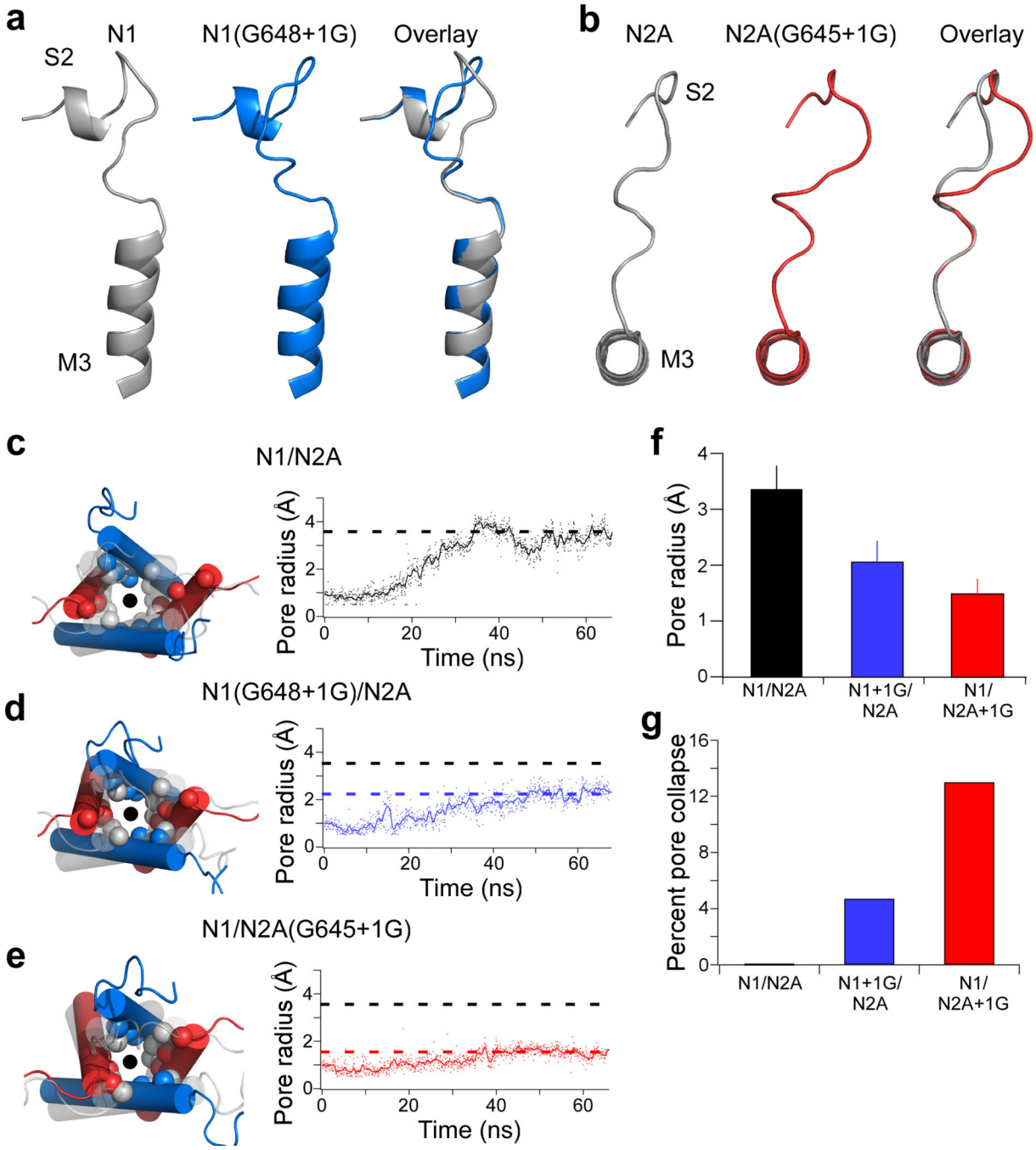

Figure 3. M3-S2 insertions attenuate pore opening in all-atom molecular dynamics simulations of modeled GluN1/GluN2A NMDARs

(**a & b**) Glycine insertions in the M3-S2 linker increase linker length. Model structures for the region around M3-S2 of GluN1(G648+1G) (**a**, *side view*) and GluN2A(G645+1G) (**b**, *top-down view*) in the resting state. Shown are M3-S2 for wild type (*left, grey*), the +1G insertion (*middle, color*), and their overlay (*right*).

(**c–e**) *Left*, Overlaid structural snapshots of the ion channel pore (circle) at 0 ns (*grey, faded*) and after 65 ns of simulation (colored) with spheres highlighting α-carbons of the three gate-

forming rings (Fig. 1e). *Right*, Change in pore radius from 0 ns to 65 ns. Shown are the filtered (line) and unfiltered (dots) traces for each construct. Dashed lines reflect average pore radius for the last 35 ns for GluN1/GluN2A (*black*), GluN1(G648+1G)/GluN2A (*blue*), and GluN1/GluN2A(G645+1G) (*red*). Pore radius was measured at the most extracellular ring formed by GluN1(V638) and GluN2A(I635).

(**f**) Mean (± standard deviation) pore radius across the final 35 ns (using 700 frames) of the MD simulations for tested constructs.

(**g**) Percent pore collapse (percent of time with pore radius < 1 Å) for each construct.

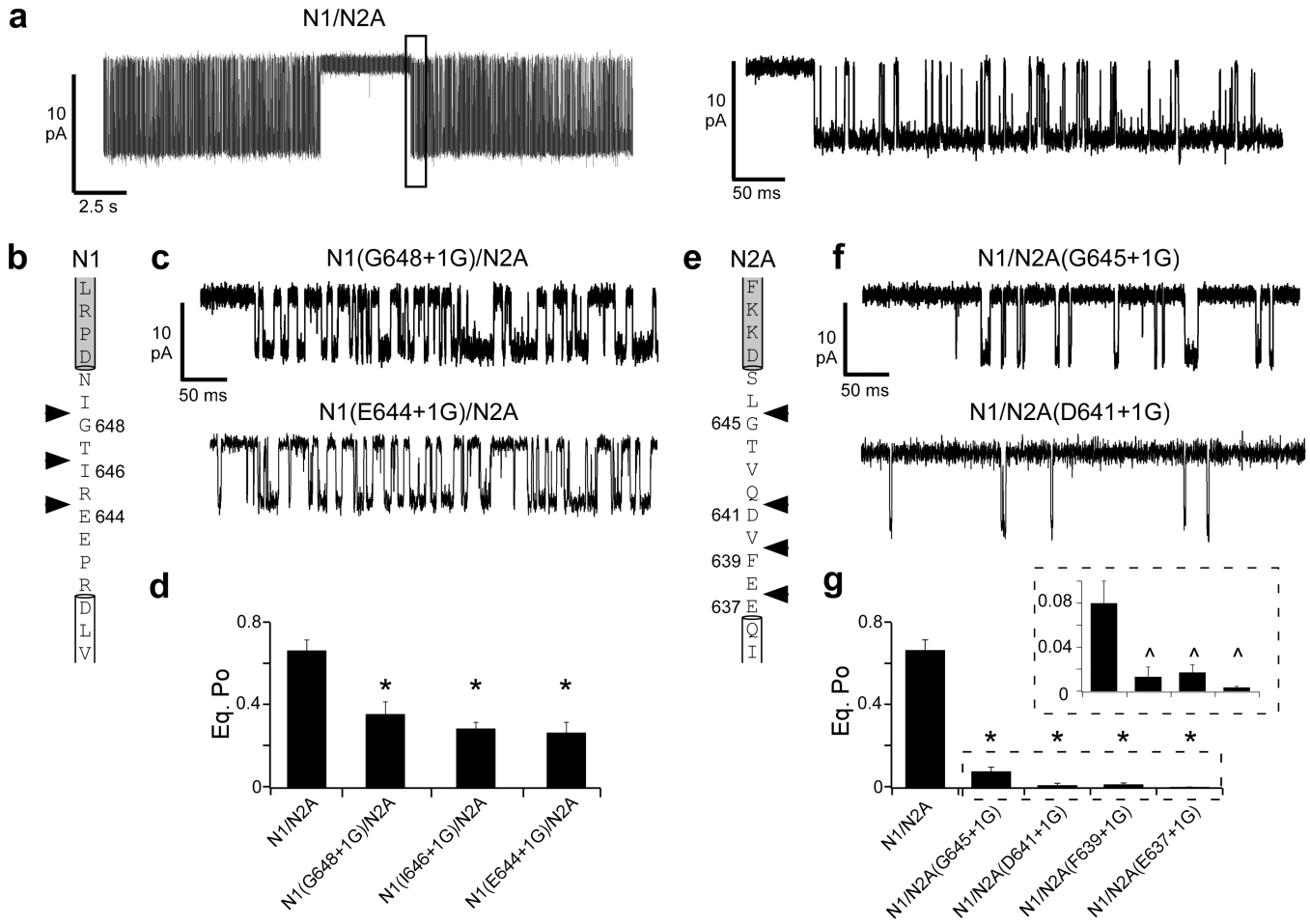

Figure 4. Insertions at different points in the M3-S2 linker attenuate pore opening

(**a**) Current traces from cell-attached patches for a single GluN1/GluN2A NMDAR at steady state either at low resolution (*left*, digitally filtered at 1 kHz) or high resolution of the boxed region (*right*, digitally filtered at 3 kHz). Patch pipettes contained saturating agonists (1 mM glutamate, 0.1 mM glycine).

(**b–d & e–g**) Glycine insertions at different points throughout the M3-S2 linker in either GluN1 (**b–d**) or GluN2A (**e–g**) significantly reduce equilibrium open probability (P_o) compared to GluN1/GluN2A.

(**b & e**) Sequence of the GluN1 (**b**) and GluN2A (**e**) M3-S2 linkers with the adjoining M3 helix (*white box*) and S2 segment (*grey box*). Arrowheads indicate points of single glycine insertions.

(**c & f**) Single channel traces (approximately 0.5 s, digitally filtered at 3 kHz) for GluN1(G648+1G)/GluN2A (**c,** *top*) or GluN1(E644+1G)/GluN2A (**c,** *bottom*) and GluN1/GluN2A(G645+1G) (**f,** *top*) or GluN1/GluN2A(D641+1G) (**f,** *bottom*).

(**d & g**) Mean (± SEM) equilibrium P_o for glycine insertions in the GluN1 (**d**) or GluN2A (**g**) M3-S2 linker. The boxed inset in (**g**) shows equilibrium P_o at a higher resolution. Significant difference is indicated either relative to GluN1/GluN2A (*) or to GluN1/GluN2A(G645+1G) (^) ($p < 0.05$, two-tailed Student's t-test, unpaired).

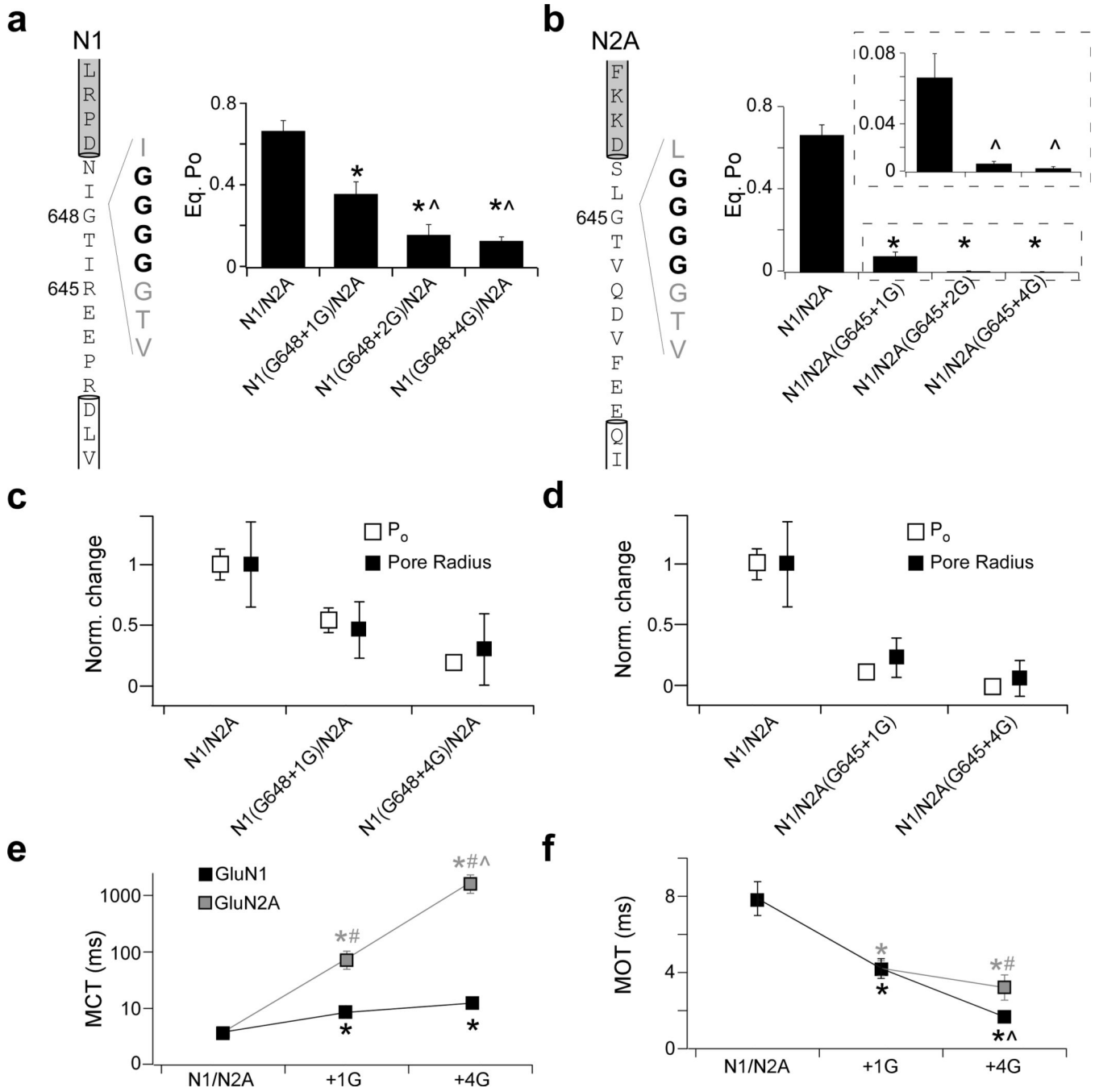

Figure 5. Additional insertions in the M3-S2 linkers further reduce pore opening

(**a–b**) *Left*, sequence for GluN1 (**a**) and GluN2A (**b**) M3-S2 linkers, with +4G insertions indicated in bold text. *Right*, mean (± SEM) equilibrium P_o for increasing glycine insertions. A significant difference is indicated either relative to GluN1/GluN2A (*) or to the respective +1G construct for each subunit (^) ($p < 0.05$, two-tailed Student's t-test, unpaired).

(**c–d**) Glycine insertions have parallel effects on pore radius (*black squares*) and P_o (*open squares*) for +1G and +4G insertions in GluN1 (**c**) and GluN2A (**d**). All values are normalized to those for GluN1/GluN2A.

(**e–f**) Insertions have subunit-specific effects on mean closed (MCT) and mean open (MOT) times. Mean (± SEM) closed (**e**) and open (**f**) time for +1G and +4G insertions for GluN1 (*black*) or GluN2A (*grey*). Note that MCT is plotted on a logarithmic scale. Significant difference is indicated either relative to GluN1/GluN2A (*), between GluN1 and GluN2A for the same manipulation ($^{\#}$), or to the respective +1G construct for each subunit (^) ($p < 0.05$, two-tailed Student's t-test, unpaired).

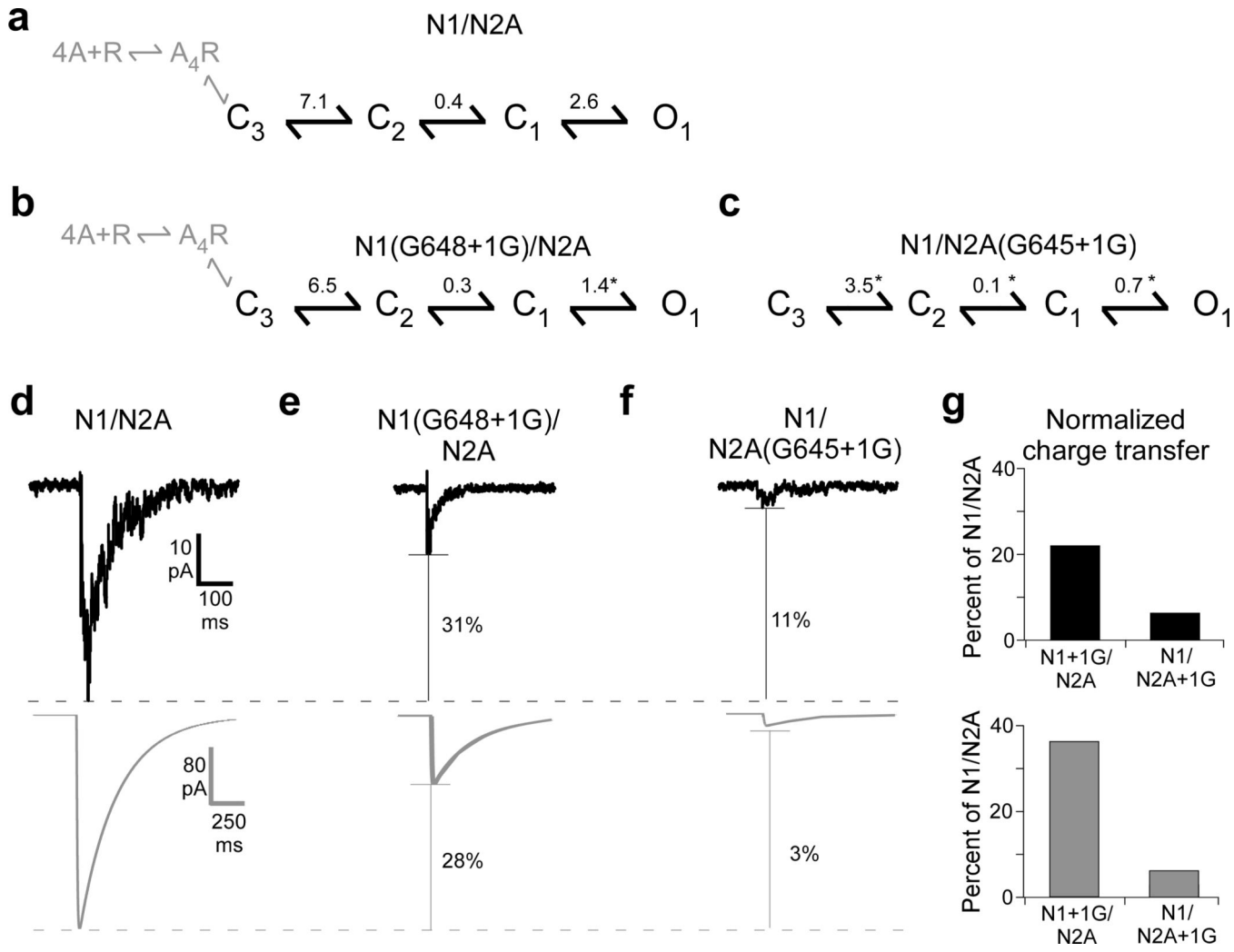

Figure 6. Activation models for single glycine insertions in GluN1 or GluN2A

All kinetic analysis was performed at a dead time of 0.024 ms.

(**a**) Kinetic schemes and equilibrium constants (Supplementary Table 4) for GluN1/GluN2A analyzed at equilibrium. Ligand binding steps are shown in grey.

(**b–c**) Kinetic schemes and equilibrium constants for GluN1(G648+1G) (**b**) or GluN2A(G645+1G) (**c**). Significant difference is indicated relative to GluN1/GluN2A (*).

(**d–f**) Simulated currents for single glycine insertion constructs parallel measured responses. *Top*, summed current profiles from Fig.1a for 2 ms glutamate applications to outside-out patches for GluN1/GluN2A (**d**), GluN1(G648+1G)/GluN2A (**e**), or GluN1/GluN2A(G645+1G) (**f**). *Bottom*, simulated current traces for the same constructs. Simulations were performed using derived kinetic rates (Supplementary Table 4) in response to a 2 ms glutamate application. Indicated for each is the % reduction in peak current amplitude.

(**g**) Charge transfer for measured (*top*) and simulated (*bottom*) currents normalized to GluN1/GluN2A.

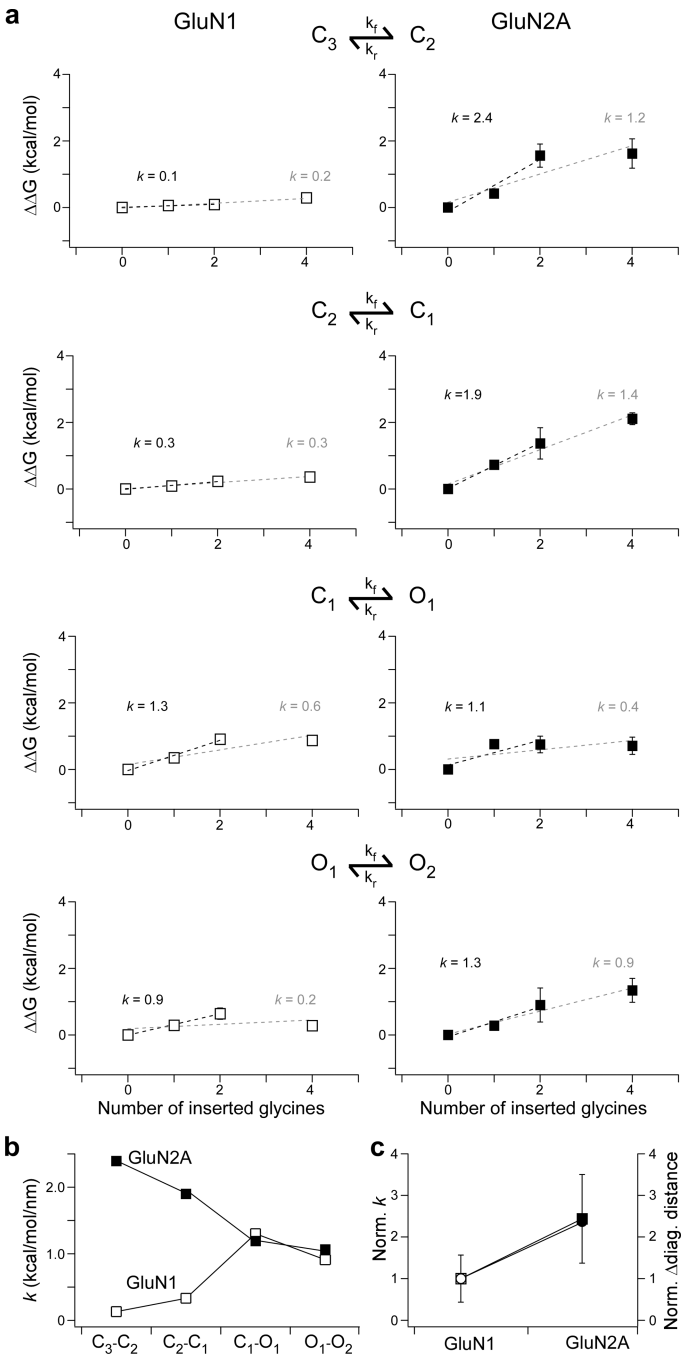

Figure 7. The GluN2A subunit moves earlier and transduces more energy than the GluN1 subunit

(**a**) The GluN2A subunit transfers more energy per unit length than GluN1. Plots correlating ΔΔG (kcal/mol) as a function of insertion length for GluN1 (*left, white*) or GluN2A (*right, black*) for the NMDAR activation transitions (C_3−C_2, C_2−C_1, C_1−O_1, O_1−O_2). Also shown is the slope (*k*, kcal/mol/nm) for linear fits to the first three (*black*) or four (*grey*) points. For subsequent analysis, we used values derived from the three-point fit due to uncertainty

whether residue insertions beyond +2G were increasing the linker length as expected (Supplementary Figs. 2 & 3).

(**b**) Pulling energetics are approximately the same during the concerted pore opening step. Summary plots for pulling energy during NMDAR activation for GluN1 (*white squares*) or GluN2A (*black squares*).

(**c**) The subunit differences in pulling energy parallel differences in pore opening. Plot for the average pulling energy (*squares*) and change in distance between like-subunit M3 helices after activation (*circles*) for GluN1 (*white*) and GluN2A (*black*). Values are normalized to GluN1. The average pulling factor was calculated assuming that the pulling factors for each transition contribute equally.

TABLE 1

Insertions in the GluN1 or GluN2A M3-S2 linker reduce channel open probability

	Total Events	*i* (pA)	P_o	MCT (ms)	MOT (ms)
GluN1/GluN2A	1,876,000 (8)	−7.9 ± 0.3	0.67 ± 0.06	3.8 ± 0.8	7.9 ± 0.9
GluN1					
G648+1G	1,760,000 (8)	−8.1 ± 0.5	0.36 ± 0.06*	8.5 ± 1.3*	4.2 ± 0.5*
G648+2G	458,000 (5)	−12 ± 1*^	0.15 ± 0.05*^	13.9 ± 3.9*	1.5 ± 0.1*^
G648+4G	598,000 (4)	−12 ± 1*^	0.13 ± 0.02*^	12.4 ± 1.8*	1.7 ± 0.1*^
GluN2A					
G645+1G	237,000 (6)	−8.2 ± 0.4	0.08 ± 0.2*#	76.2 ± 27*#	4.2 ± 0.4*
G645+2G	14,100 (5)	−9.5 ± 1.6	0.008 ± 0.002*^#	620 ± 80*^#	5.1 ± 1.4
G645+4G	12,300 (6)	−11.5 ± 0.8*	0.003 ± 0.001*^#	2300 ± 600*^#	3.7 ± 0.4*#

Mean values (± SEM) for single-channel current amplitudes (*i*), equilibrium open probability (P_O), mean closed time (MCT), and mean open time (MOT) for wild type and insertion constructs in GluN1 or GluN2A. Single-channels data was recorded in the cell-attached configuration and analyzed in QuB. Number of patches is in parenthesis to the right of total event numbers. Significant difference is indicated either relative to GluN1/GluN2A (*), to the respective +1G construct for each subunit (^), or between GluN1 and GluN2A for the same mutation (#) ($p < 0.05$, two-tailed Student's t-test, unpaired).